Available online at www.sciencedirect.com
SCIENCE DIRECT®
C. R. Physique 4 (2003) 975–991
COMPTES RENDUS PHYSIQUE

Carbon nanotubes: state of the art and applications/Les nanotubes de carbone : état de l'art et applications

Nucleation and growth of SWNT: TEM studies of the role of the catalyst

Annick Loiseau [a,*], Julie Gavillet [a], François Ducastelle [a], Jany Thibault [b], Odile Stéphan [c], Patrick Bernier [d], Saïd Thair [d]

[a] *LEM, Onera-CNRS, 29, avenue de la Division Leclerc, BP 72, 92322 Châtillon, France*
[b] *CEA-Grenoble, département de recherche fondamentale sur la matière condensée, 17, rue des Martyrs, 38054 Grenoble, France*
[c] *Laboratoire de physique des solides, bâtiment 501, 91405 Orsay, France*
[d] *GDPC, Université Montpellier II, CC026, place Eugène Bataillon, 34095 Montpellier, France*

Presented by Guy Laval

Abstract

This paper reviews transmission electron microscopy studies, combining high resolution imaging and electron energy loss spectroscopy, of the nucleation and growth of carbon single wall nanotubes with a particular emphasis on the nanotubes obtained from the evaporation-based elaboration techniques. Inspection of samples obtained from different synthesis routes shows that in all cases nanotubes are found to emerge from catalyst particles and that they have grown *perpendicular* or *parallel* to the surface according to whether they have been synthesized via evaporation-based methods or CCVD methods. Whereas the latter case corresponds to the well-known situation of carbon filaments growth, the former case strongly suggests another formation and growth process, which is described and its different steps discussed in detail. In this model, formation of the nanotubes proceeds via solvation of carbon into liquid metal droplets, followed by precipitation, at the surface of the particles, of excess carbon in the form of nanotubes through a nucleation and root growth process. It is argued that the nucleation of the nanotubes, which compete with the formation of graphene sheets wrapping the surface of the particle, necessarily results from a surface instability induced by the conditions of segregation. The nature and the origin of this instability was studied in the case of the class of catalyst Ni–R.E. (R.E. = Y, La, Ce, ...) in order to identify the influence of the nature of the catalyst. The respective roles played by Ni and R.E. have been identified. It is shown that carbon and rear-earth co-segregate and self-assemble at the surface of the particle in order to form a surface layer destabilizing the formation of graphene sheets and providing nucleation sites for nanotubes growing perpendicular to the surface. ***To cite this article: A. Loiseau et al., C. R. Physique 4 (2003).***

Résumé

Germination et croissance des nanotubes monofeuillets : études par microscopie électronique en transmission du rôle du catalyseur. Cet article présente une revue des études, par microscopie électronique en transmission, couplant imagerie de haute résolution et spectroscopie de pertes d'énergie d'électrons, de la germination et de la croissance des nanotubes de carbone simple feuillet, avec un développement particulier pour les tubes obtenus par les techniques de synthèse mettant en jeu la vaporisation d'une cible. L'examen d'échantillons provenant de différentes voies de synthèse montre que, dans tous les cas, les nanotubes émergent de particules catalytiques et qu'ils ont crû perpendiculairement ou parallèlement à la surface selon qu'ils ont été synthétisés par des méthodes mettant en jeu la vaporisation d'une cible ou des méthodes de type CCVD. Alors que le dernier cas correspond à la situation bien connue de la croissance des filaments de carbone, le premier cas suggère fortement un autre procédé de formation et de croissance, qui est décrit et ces différentes étapes discutées en détail. Dans ce modèle, la

* Corresponding author.
E-mail address: Annick.Loiseau@onera.fr (A. Loiseau).

1631-0705/$ – see front matter
doi:10.1016/j.crhy.2003.10.022

formation des tubes s'effectue par dissolution de carbone dans des gouttes de métal liquide, suivie de la précipitation, à la surface des particules, du carbone en excès sous la forme de nanotubes par un mécanisme de nucléation et de croissance par le pied. Il est démontré que la nucléation des nanotubes, qui est en compétition avec la formation de feuillets de graphène couvrant la surface de la particule, provient nécessairement d'une instabilité de surface induite par les conditions de ségrégation. La nature et l'origine de cette instabilité a été étudiée dans le cas de la classe de catalyseurs Ni–R.E. (R.E. = Y, La, Ce...) afin d'identifier l'influence de la nature du catalyseur. Les rôles respectifs joués par le Ni et la terre rare ont été identifiés. Il est montré que le carbone et la terre rare co-ségrègent et s'auto-assemblent à la surface de la particule de façon à former une couche de surface qui déstabilise la formation de feuillets de graphène et qui est source de sites de nucléation pour des nanotubes croissant perpendiculairement à la surface. ***Pour citer cet article : A. Loiseau et al., C. R. Physique 4 (2003).***

1. Introduction

Carbon single-wall nanotubes (C-SWNTs) are produced via techniques running at either high temperatures (arc discharge [1], laser ablation [2], laser vaporization [3] and solar furnaces [4]) or at medium temperatures (CVD based methods) [5–7], which all involve a metal catalyst. In the high temperature evaporation based-route, carbon and metallic elements (Co, Ni, Y, La, ...) are vaporized at temperatures above 3000 K and then condensed at lower temperatures in an inert gas (He, Ar) flow and single wall nanotubes are believed to form at about 1500 K. In particular, the use of a pulsed laser in the laser ablation method requires placing the reactor in an oven heated at least 1300 K to obtain significant yields in SWNT. The catalytic CVD (CCVD-) based routes use the decomposition of an hydrocarbon gas (methane, ethylene, ...) or of CO at the surface of catalytic particles (Fe, Co, Ni) which are either deposited on a substrate or synthesized in situ from a solid or liquid precursor and sprayed in the furnace. Depending on the temperature, different products are obtained. Although there is no general rule, the tendency is to obtain multi-wall nanotubes at temperatures ranging from 500 to 900 °C and single-wall nanotubes at higher temperatures (750–1200 °C) [8].

The analogies between these fairly different methods are actually remarkable [8]: First, the morphologies of the SWNTs produced by the different techniques are very similar. In each case, SWNTs can be found isolated or self-assembled in crystalline bundles, their diameter varying from 0.7 to 3 nm. These correlations suggest that a common mechanism could explain the growth of SWNTs. Second, for all synthesis techniques, catalysts such as Ni, Co, Fe, Y, La or mixtures of them are necessary to obtain SWNTs. Several questions then arise which concern the role played by the temperature and the metallic catalyst: is the catalyst active at the atomic level or as a cluster, in a liquid or a solid state and through which catalytic reaction processes?

In nanotubes, carbon has a structure which is not very different from its most stable structure at equilibrium, i.e., graphite. Nanotubes can therefore be considered as particular microstructures of sp^2 carbon. The understanding of their formation requires then an analysis of the kinetic transformation paths of carbon from the vapour to the solid state which themselves depend on the phase transformations involved in the catalyst-carbon systems. This means that understanding the nanotube formation implies an examination of the different microstructures which can result from these transformations. From an experimental point of view two types of methods are used. The structural determinations and chemical analyses of the synthesis products are made ex situ after the synthesis using local or global probes techniques (for a review see, e.g., [9]) whereas in situ diagnostics in evaporation-based synthesis reactors are now becoming available [10–14]. Among the techniques used in post synthesis analyses, transmission electron microscopy (TEM) plays a major role, since it is the only technique able to provide information in imaging, diffraction and chemical spectroscopy modes [8,9]. In situ diagnostics inspect the temperature, nature of species issued from the target vaporization, time scales in pulsed laser reactors and residence time in continuous vaporization processes. From a theoretical point of view, thermodynamic treatments at the mesoscopic level [15–17] as well as atomistic modelizations (starting from ab initio or empirical interatomic potentials) [18–20] have been developped.

Although the situation is not yet completely clear, some realistic scenarii begin to emerge from these different approaches [21]. The paper will focus here on the TEM investigations we have undertaken and developed in the recent years [22] and on microscopic modelizations with a particular emphasis on the growth of nanotube bundles emerging from catalyst particles obtained from the evaporation-based routes. TEM identification and comparison of the microstructures arising from different synthesis routes are first presented in Section 2, where it will be shown that the observations support a general phenomenological model of SWNTs nucleation and growth and that the arguments of this model are confirmed by ab initio calculations. The specific case of the R.E.–Ni class of catalysts (R.E. = Y, La, Ce) is then discussed in detail in Section 3.

2. Towards a general phenomenological model of nucleation and growth

2.1. SWNTs morphologies

Since samples generally consist of a mixture of metallic particles and of an entangled network of nanotubes, isolated or assembled into bundles. First observations have concerned the identification of the relationships between particles and bundles. High resolution transmission electron microscopy (HRTEM) analyses indicate that, actually, whatever the synthesis process, SWNTs nucleate and grow from the catalytic particles [19]. In particular, we have performed careful and systematic HRTEM studies using a JEOL 400FX working at 400 kV of SWNTs extremities of samples produced by arc discharge [1], laser ablation [2], laser vaporization [13,23,24] and catalytic decomposition [7,25]. The observations, shown in Figs. 1–3, have also been compared with those made on samples obtained by solar energy [4]. In all cases, it is found that the nanotubes are attached by one extremity to small (5–20 nm in diameter) metallic particles although differences in the size of the particles, in the number of tubes per rope and in the crystallinity of the tubes are evident. The situation where the nanotubes are short (<400 nm) is of particular interest since both tube extremities can be observed simultaneously, which is quite impossible for long tubes because of their entanglement: in these cases (Fig. 2 and Fig. 1(f)), it is clearly seen that one tube extremity is attached to the particle and the other is closed and empty. The situation shown in Fig. 2(d), where numerous bundles corresponding to several tens of SWNTs emerge radially from a given particle, is called a sea urchin structure and has been observed for different catalysts [4, 26,27]. Finally, very short tubes corresponding to bundle embryos or nuclei have been clearly identified and different situations are shown in Fig. 3. Fig. 3 (a) and (e) show bundle embryos whereas in the other cases a single nanotube is emerging from the particle.

It results from these observations that there are basically two situations. In the first case the tube growth is *perpendicular* to the surface of the particle. This is the general situation encountered in the evaporation based route, where the particle are fairly large (5–20 nm) (Fig.1(a), (d)–(f) and Fig. 3(a)–(c), (e)) (see also [28]) but it is sometimes observed in CCVD samples (see Fig. 1(b)) [7]. In this growth mode, the tubes are most frequently arranged in bundles (see Fig. 1(a), (b), (d)) but single tubes emerging perpendicular to the surface of the particles can also be observed as in Fig. 3(b)–(d). In such cases, the diameters of the tube are *not* correlated with the size of the particle. In the second case, the growth is *tangential*; the particles are generally smaller (1–5 nm) and are found encapsulated at the tip of the tubes (Figs. 1(c) and 3(f)), thus determining their diameter. Many other examples can be found in the literature, as for instance in [5]. This growth process has, to our knowledge, only be observed in the CCVD methods.

2.2. Model of nucleation and growth

The tangential growth process, observed for CCVD SWNTs, should be similar to those put forward to explain the growth of carbon filaments (Fig. 4(a)) [29–31]: the nanotubes can be considered in this case as ultimately small carbon filaments (Fig. 4(b)) [5]. The process, sketched in Fig. 4, involves a chemisorption and decomposition of the carbonaceous gas at the surface of the particle, the dissolution and the diffusion of carbon within the particle and its segregation and graphitization parallel to the surface of the particle, once the particle gets saturated in carbon. The carbon concentration gradient between the surface and the bulk of the particle insures the continuity of the process, as long as the temperature and gas supply, at a rate avoiding the catalyst poisoning, are maintained. The diameter of the tube emerging from the graphitization process is naturally determined by the size of the particle which, during the growth, can either be rejected at the tip or be kept at the foot of the tube and attached to the support.

Such a process, however, fails to take into account the situation, typical of the vaporization routes, where the growth is perpendicular to the particle. Different alternative models have been tentatively proposed in the recent years. First, a direct formation process in the gas phase has been considered [2]: catalyst acts through aggregates reduced to a few atoms located at the tip of the nanotube, either preventing its closure by scooting around and stabilizing the reactive dangling bonds or leading the tip to remain chemically active [20] or stabilizing structural defects and acting as attraction sites for carbon adatoms [32]. Other models involve the growth from a liquid metallic particle, the SWNT nucleation step being a highly debated issue. It has been suggested, in particular, that preformed fullerenes could play the role of nucleation seeds [33].

On the basis of the TEM observations described above, we have developed a simple model [8,19], which adopts the concepts of the so-called VLS (vapor–liquid–solid) model introduced for explaining the growth of silicon whiskers [34]. This model was first adapted by Saito et al. [26], for explaining the formation of sea-urchin-like structures. Here we extend the VLS approach to the formation of both individual SWNTs and SWNTs bundles, which are emerging perpendicular from the particle. In this type of model, the growth of nanotubes is believed to proceed via solvation of carbon vapour into metal clusters, followed by the precipitation of carbon excess in the form of nanotubes. The mechanism is based on the ability of metals such as Ni, Co to dissolve carbon when liquid and to almost completely segregate upon solidification, therefore allowing graphitization of carbon

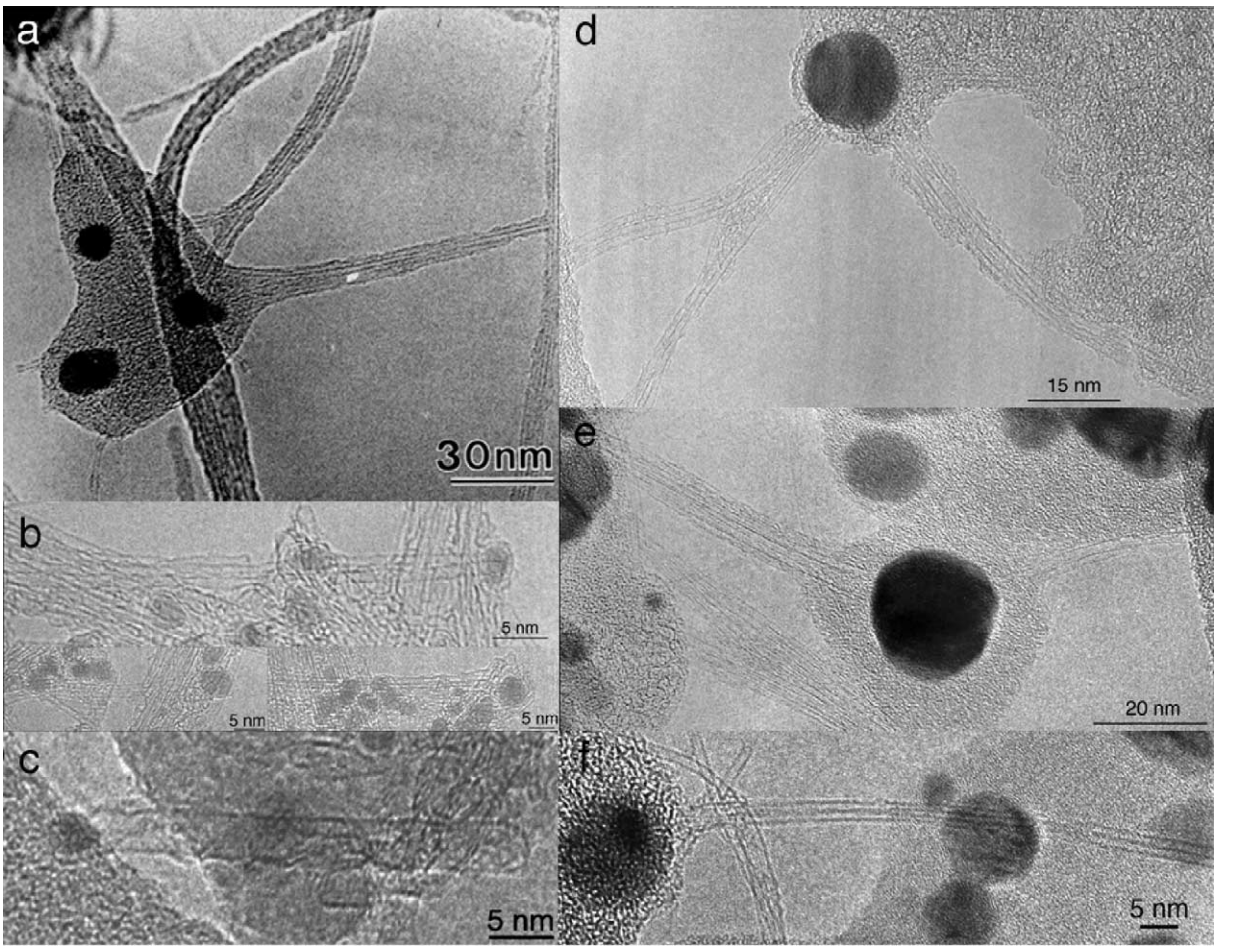

Fig. 1. HRTEM images (Jeol 4000FX, Cs = 3.2 mm)) of long SWNTs ropes emanating from metallic particles synthesized by various methods: (a) electric arc discharge described in [1] with a Ni–Y catalyst where the Y/Ni ratio is equal to 0.2; (b) HIPCO CCVD process described in [25]; (c) CCVD procedure described in [7]; (d) pulsed laser ablation described in [2]; (e) and (f) continuous laser vaporization described in [23]. Note that in (b) the particle size is much smaller than in the other cases and that the ropes contain a reduced number of tubes. When the particle is large ((d), (e)), two ropes or more can emerge from it. Furthermore, it is frequently observed, as it can be seen in (a), that bundles issued from distinct particles attract each other according to a branching process and form a composite rope [48]. Finally, note that in (c) the diameter of the tube is related to that of the particle in contrast with the situations shown in the other cases.

at temperatures as low as 1500 K [35,21]. The parentage with the models mentioned above for the tangential growth is obvious since they are based on thermodynamical properties of catalyst (Ni, Co)–carbon systems.

Fig. 5 presents a simplified sketch of the proposed scenario. The first step (Fig. 5(a)) of the process is the formation of a liquid nanoparticle of metal supersaturated with carbon. These nanoparticles originate from condensation of the metal plasma/vapour in the moderate temperature zone of vaporization based reactors. Upon cooling, the solubility limit of carbon decreases and carbon atoms segregate towards the surface where they precipitate. The second step (Fig. 5(b), (c)) is the formation of nanotube nuclei at the surface of the particle which is competing with the formation of a graphitic sheet wetting the surface of the particle. The last step (Fig. 5(d)–(f)) is the nanotube growth which is likely to proceed by a progressive incorporation of carbon at the interface particle-nanotube. This scenario, which implies a root growth mechanism, is supported by the different TEM observations presented in Section 2.1, for the nucleation step at least, and by ab initio calculations [19], whereas in situ diagnostics performed in laser methods [10,12,14,36] and solar furnaces [37] provide information consistent with the first step. We discuss below in more details these different steps with a particular attention to the nucleation one which is the most crucial.

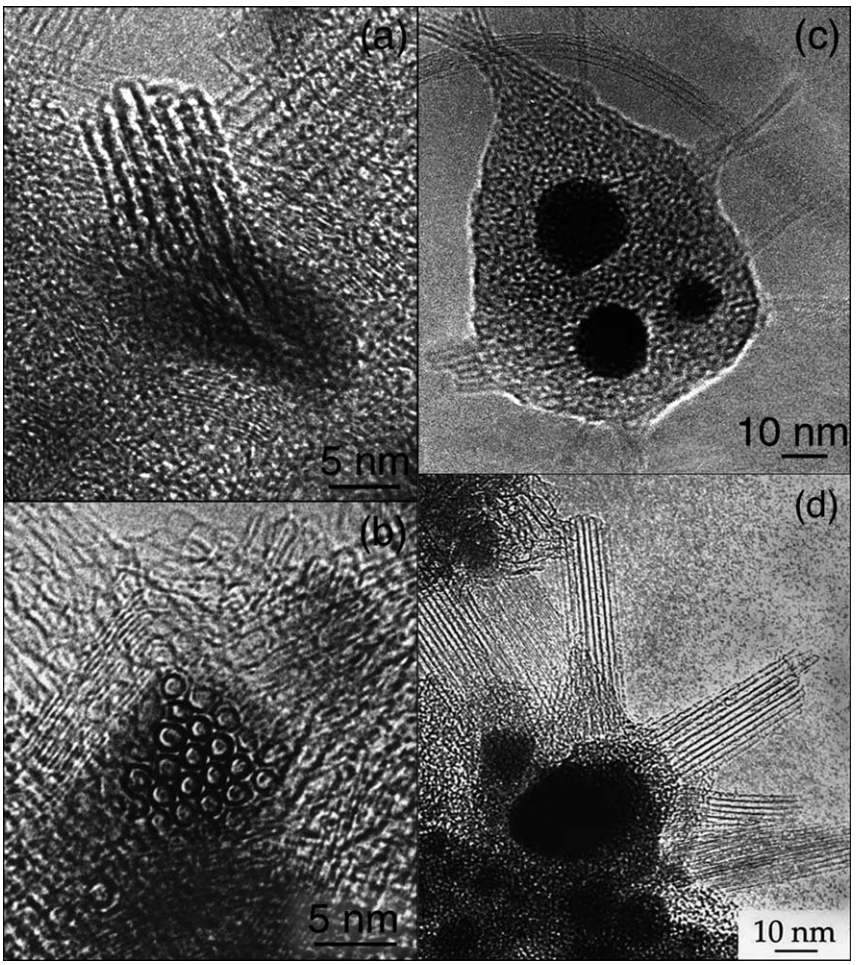

Fig. 2. HRTEM images of different short ropes attached to the metallic particles. Samples are synthesized with the electric arc and with a Ni–Y catalyst where the Y/Ni ratio is equal to 0.5. In (a) the rope is strongly inclined with respect the electron beam and in (b) it is perpendicular to it. In (c) the ropes and the particles are embedded in an amorphous carbon flake. In (d) different ropes are emerging radially from the particle in different spatial directions reminding to a sea-urchin hence the name given to these morphologies.

2.3. Particle formation and carbon segregation

The presence of metal atomic vapours and of C_2 molecules is attested by the in situ diagnostics [10,12,14,37] done in continuous and pulsed vaporization reactors. As expected from thermodynamic data, carbon condenses first. In pulsed laser reactors, the signal corresponding to the metallic vapour disappears ten times later than the C_2 signal. Because of the high quenching rate, expected to be 10^5–10^6 K/s from continuous laser reactor [14] and solar furnace [36], carbon condenses in a low density amorphous state. Neither graphite nor diamond crystallites have been detected in the synthesis products. From in situ measurements [12,14], metal condenses below 2300–2000 °C, resulting in the formation of liquid particles (Fig. 5(a)). The nanoparticle size is determined by parameters such as temperature gradients, gas pressure and flow, etc. [24,38,39]. These particles can dissolve a substantial amount of carbon, up to 25 at.% at 2000 °C after the thermodynamic data and probably much more, up to 50–60% [40], when the particles are very small. Ni–C and Co–C phase diagrams [35] indicate that the solubility limit drastically decreases down to a few at.% as the temperature is falling down to the eutectic temperature ($T = 1400$ °C), where the metal solidifies. The solidification gives rise to a phase separation between an almost pure metallic phase and a solid pure carbon phase. The phase separation proceeds by a segregation of carbon towards the surface of the metallic particle because of two combined effects: the drastic difference in energy of the respective surface tensions of metals and carbon [21] and the reduced particle size. This phenomenon of surface segregation has been confirmed by ab initio calculations done in the Co–C system [8,19].

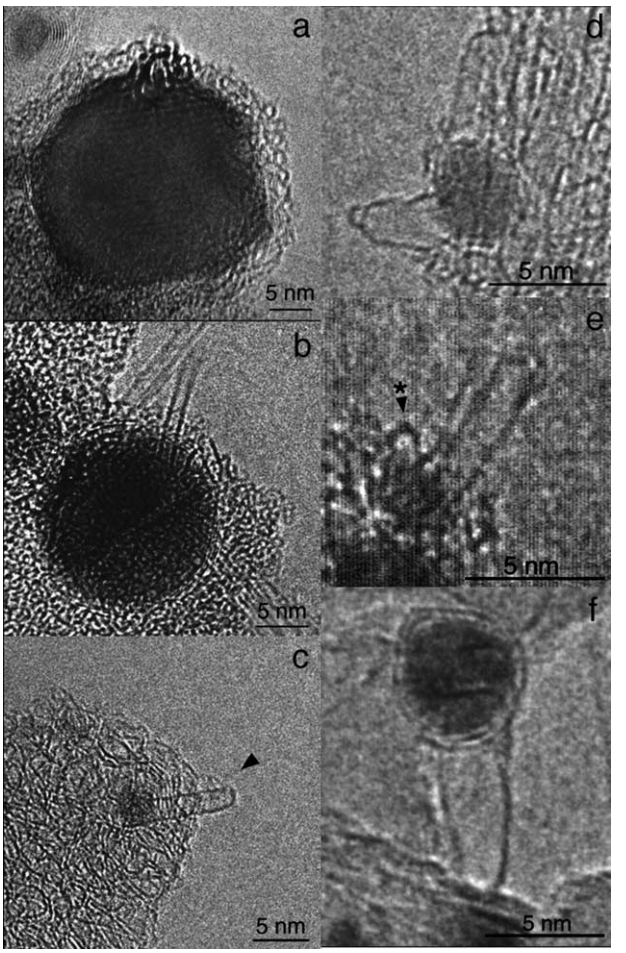

Fig. 3. HRTEM images of embryos of SWNTs emerging from metallic nanoparticles. Nanotubes are synthesized by electric arc discharge [1] in (a), (b) and (c), by the HIPCO process [25] in (d), (e) and by the CCVD process described in [7] in (f)). In each case, the nanotubes are seen as elongated caps having a length between 3 and 5 nm. The images (a) and (e) show embryos of a SWNT bundle, whereas in the other cases, only one nanotube is emerging from the particle whose size is not correlated to that of the tube except in (f). It is worth noticing that, in this particular case, the graphitic walls of the tube are tangent to the surface of the particle, whereas in the other cases, the tubular sheets are perpendicular to the particle surface.

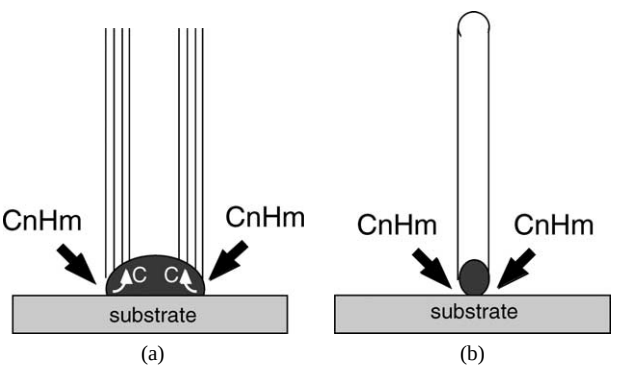

Fig. 4. (a) Simplified schema for the formation of carbon filaments obtained from CCVD methods [29–31] and its adaptation to the formation of SWNT growing tangentially to the surface of the particle in (b) [5].

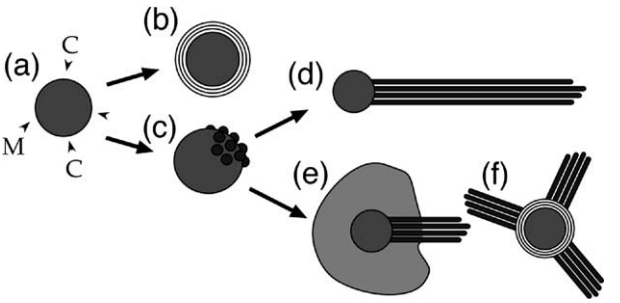

Fig. 5. Scenario derived from the VLS model, for the nucleation and growth of SWNT.

2.4. Nucleation

Once expulsed, carbon crystallizes at the surface of the particle according to two competing transformation paths (Fig. 5(b), (c)), which lead either to graphene sheets wrapping the particle and wetting its surface or to SWNTs nuclei with graphitic walls perpendicular to the surface, that is, nonwetting it. Since equilibrium surface energy arguments play in favour of the first configuration [21], it has to be assumed that the SWNTs nuclei result from a particular surface process, for which the graphene sheet becomes unstable. As explained above, the segregation force increases upon cooling and is maximum close to solidification. If the segregation velocity is low, carbon can be progressively and gently extruded in such a way that carbon atoms get organized by surface and bulk diffusion in the most stable configuration, that is, the graphene sheet. On the other hand, when the segregation velocity is high, the carbon flux is too rapid to permit, by diffusion, progressive incorporation of atoms at the edges of a graphene layer and because of this conflict surface instabilities occur.

The precise nature of these instabilities is for the moment a debated issue, discussed in detail in [21]. One can imagine dynamic instabilities as those involved in the formation of dendrites in solidification processes [41] or quasi static instabilities similar to those involved in crystal growth produced by molecular beam epitaxy deposition [42]. The latter analogy is very appealing indeed if one replaces the deposition flux by a segregating carbon flux. The equivalent of a layer-by-layer growth (or Frank–van der Merwe process) would be here the formation of graphene sheets whereas the formation of islands (Volmer–Weber or Stranski–Krastanov processes) would be equivalent to the growth of nanotubes (for details see [21]). The limit of these analogies lies in the difference in scales compared to the length and the diameter of the nanotubes: macroscopic size of the dendrites in the first scale, nanometer height of the islands in the second case. In all cases, the instability is governed by two control parameters: one is the surface energy and the second one can be, in turn, depending on the system, a kinetic energy as in dendritic solidification, a concentration gradient, or elastic and chemical energies which determine the wetting properties of the surface. In our case, the carbon surface tension is clearly one parameter, whereas the second one should be related to the chemical nature of the catalyst and to the kinetic conditions of cooling. In particular, the surface layer of the catalyst should have a particular structure and chemistry in such a way that its energy becomes unfavourable to the wetting of the graphene sheet, which is a condition required for the SWNTs nucleation. We will see, in Section 3, how this condition is achieved in the case of the Ni–R.E. catalyst. Finally, since the nucleation of bundles can occur, the instability should be cooperative in order to explain the collective formation of an assembly of nanotubes. Recent observations done on bundles produced by CCVD [43] methods indicate that, for small bundles, all the tubes have the same helicity, attesting for a cooperative nucleation process.

2.5. Growth and end of the growth

Once the nanotube nuclei are formed, growth should proceed through further incorporation of carbon. Carbon initially dissolved in the particle should continue to condensate at the root but this is not sufficient to produce long (one micron ore more) SWNTs bundles [8]. For instance, a nanoparticle of 15 nm in diameter and containing initially 50 at.% C can give rise to either one SWNT of 1 micron long or to a bundle of ten SWNTs of 100 nm each [8]. Another source is therefore necessary, which is naturally the density of the remaining amorphous carbon. The incorporation of this carbon can follow the dissolution-process based on a concentration gradient within the particle and invoked in the growth of filaments in CCVD methods, or can directly be incorporated at the root of the nanotubes. Semi-empirical simulations have shown the presence of reactive sites, such as pentagons, at the foot of a SWNT nucleus, enabling the incorporation and rearrangement of new carbon atoms [18]. Furthermore, this root mechanism has been observed to be very efficient in ab initio calculations [19]. One cannot exclude that a small amount of carbon is incorporated at the tip with the assistance of at least one metal atom located at the tip, acting as attraction sites for carbon adatoms [20,32]. Although this process has to be considered, it is certainly not the main one.

In order to achieve long nanotubes (Fig. 5(d)), the growth should therefore continue for a sufficient long time, as attested by in situ diagnostics and post synthesis annealing experiments [12], until local temperatures are too low, leading to the solidification of the nanoparticles. These conditions define a kind of stationary regime where the kinetics of incorporation of carbon in the tube walls is compatible with the cooling kinetics and the carbon supply. These constraints certainly explain the necessity of using in the pulsed laser reactor an oven heated at around 1500 K, that is at a temperature close to the metal solidification temperature [2,44,45]. Such an oven is not necessary in continuous vaporisation methods [3,4,14,46], since in this case the carrier gas is heated in the vicinity of the target and acts as a local furnace. In the case of the continuous laser vaporization, in situ measurements of the temperature of the carrier gas have shown the existence of a temperature plateau around 1200 K, located at a distance of few mm from the target surface (the reactor is vertical and the carrier gas is flowing from the bottom to the top of the reaction chamber [23,24]), which is suitable for the growth of long ropes [14].

Different morphologies can arise, which are sketched in Fig. 5(e), (f), when the local conditions have been perturbed in such a way that the growth has stopped. According to the root growth process, looking at the feet of the nanotubes provides information on the end of the growth, and how this has been perturbed, before stopping. The remaining carbon, which was immediately available for the growth, can partly condense into amorphous carbon flakes embedding the particle (examples can be seen in Fig. 1 and in Fig. 2(c)) or into a few graphitic layers wrapping the particle and building a buffer layer between the nanotubes and the particle (examples can be seen in Fig. 2). The former case (Fig. 5(e)) suggests a rapid decay of the local

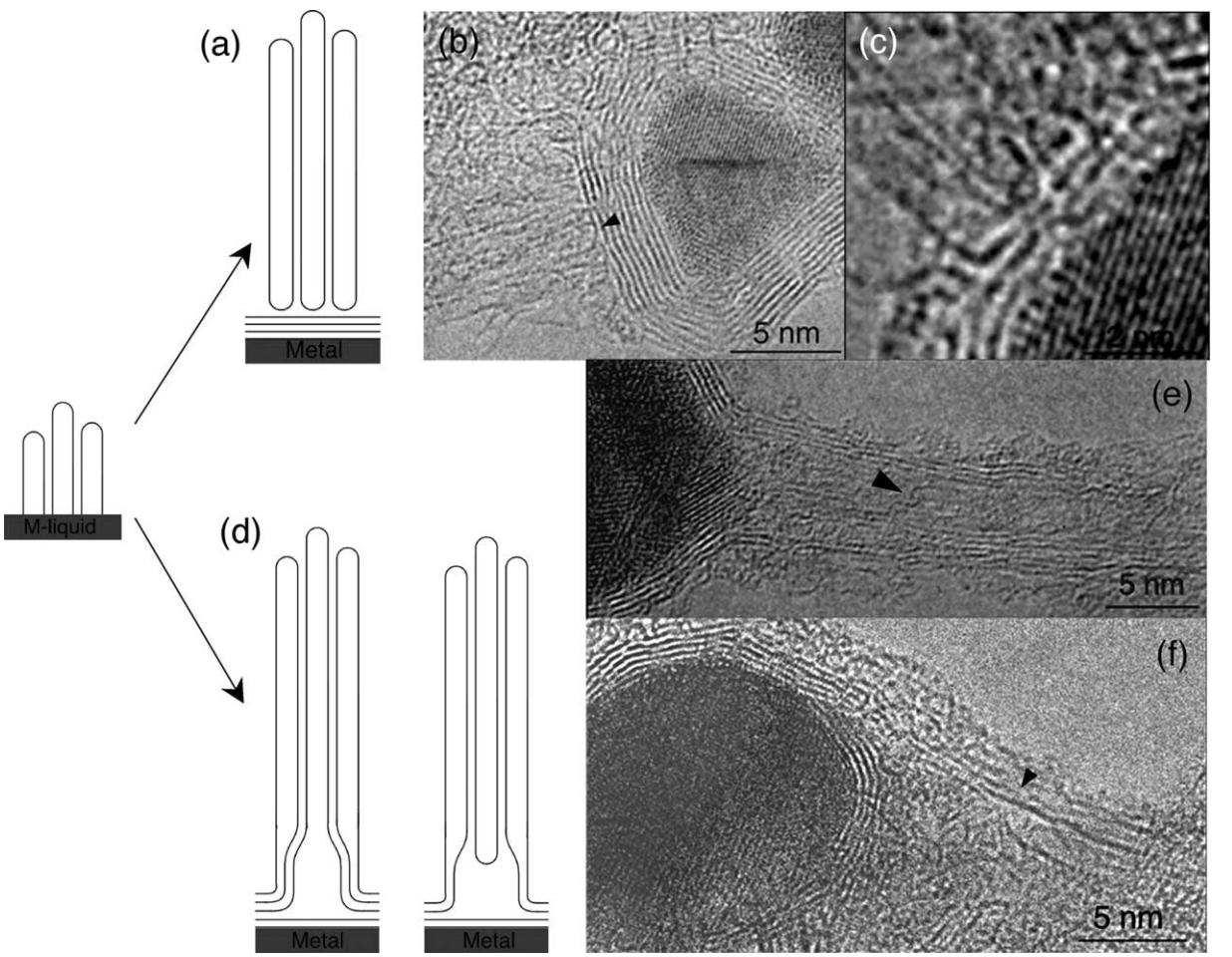

Fig. 6. Analysis of the different morphologies of SWNT feet and of their interface with the particle. Nanotubes are obtained from the electric arc [8]. (a) Schema of the situation shown in the HRTEM (Jeol 4000FX) image in (b). The image in (c) is a magnification of the area indicated by the arrow in (b). (d) Scheme of the situations shown in the HRTEM images in (e) and (f), where SWNTs of a rope are transformed into a MWNT. The arrow in (e) indicates the closure of a SWNT surrounded by a MWNT, which corresponds to the right-hand side schema of (d). The arrow in (f) indicates the constriction of a SWNT leading to its transformation into a layer of the MWNT. Note the continuity of the layers of the MWNT and of the graphene sheets wrapping the particle.

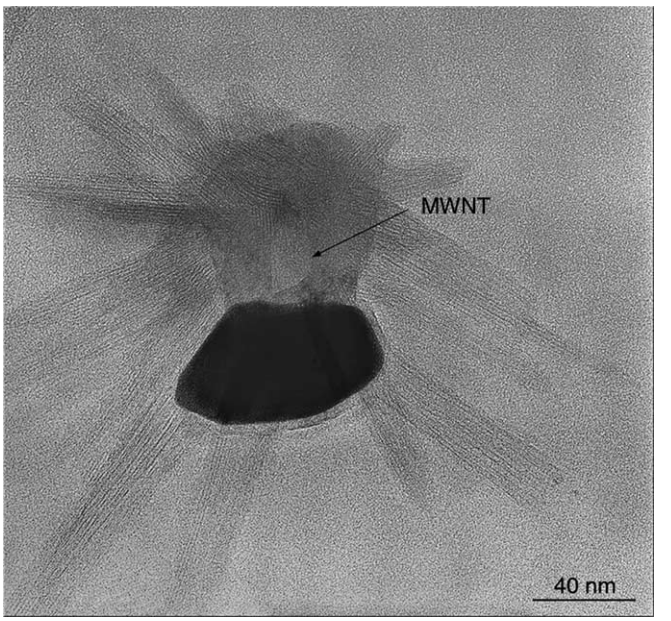

Fig. 7. HRTEM image of a particle of Pd which has generated a sea-urchin structure and a short MWNT successively. The sample is obtained from the electric arc [8].

temperature whereas the latter situation (Fig. 5(f)) means the occurrence of a bifurcation from the nanotube growth towards the continuous layer growth. This bifurcation is an additional proof that nanotubes and graphitic layers do not occur for the same local conditions of carbon segregation. We have examined very carefully numerous nanotubes feet in order to identify if the bifurcation is abrupt or progressive, in which case configurations intermediate between the nanotube and the graphitic shell could exist. Two kinds of situations have indeed be identified which are analysed in Fig. 6. Fig. 6(a)–(c) corresponds to the first case with a sharp interface between the two graphitic structures, where the tubes are closed and do not display any junction with the outer layer of the graphitic shell. On the other hand, the situation analysed in Fig. 6(d)–(f) defines a progressive bifurcation since single wall nanotubes are observed to transform, trough a complex process sketched in Fig. 6(d), into a kind of a multi-wall nanotube where the walls are connected continuously to the layers wrapping the particle.

The growth of multi-wall nanotubes from catalytic particles is a well-known process in CCVD methods and can also be obtained from evaporation based routes [47]. The present observations strongly suggest that, when assisted by a metallic catalyst, the formation of a MWNT also proceeds from a dissolution-segregation process but requires conditions of carbon segregation and diffusion intermediate between those required for SWNT and continuous layers. An additional proof of the validity of the model is provided by the configuration shown in Fig. 7. In that case, obtained from the electric arc (catalyst is Pd), particles, which have first generated SWNT in a sea-urchin structure, have been expulsed from the core of the sea-urchin and have then generated a short MWNT. Different morphologies can thus emerge from a same particle provided that the local experimental conditions suited for their growth are successively achieved.

3. Microscopic approach of the nucleation: the case of the Ni–R.E. catalysts

3.1. Experimental equipment

The nucleation step, discussed in Section 2.4, has been investigated in detail in the case of the Ni–(R.E. = Y, Ce, La) catalysts by examining the structure and the composition of the particles linked to the different SWNTs morphologies. We focused on this particular class of catalysts since they are preferentially used in continuous vaporization routes such as the arc discharge method [1] and the continuous laser reactor [3,24]. It has indeed been recognised that the highest SWNT production rate is achieved when a few amount of a rear earth element such as Y is added to the transition metal catalyst.

To study the influence of the R.E. addition on the SWNT formation, we have studied different rare earth elements – Y, Ce, La – with different compositions (from 0 to 100%). SWNTs were synthesized by the arc discharge method at the GDPC with the conditions given in [1]. The structure and the chemistry of the particles linked to the different SWNTs morphologies have

been studied by combining different TEM and scanning-TEM (STEM) modes. Fine structural studies requiring HRTEM have been performed on a JEOL 4000FX (Cs = 2.3 mm), JEOL 4000EX (Cs = 1 mm) and a JEOL 3010 (Cs = 0.6 mm). Global chemical analysis of the particles was achieved by X-ray analysis on a Philips CM20 equipped with EDX. Spatially resolved chemical studies were based on the electron energy loss spectroscopy (EELS) and have been performed both on the JEOL 3010 equipped with a GIF (Gatan Imaging Filter) providing energy filtered images (EFTEM) and on the STEM-VG501 using the 2D-line EELS spectrum mode.

3.2. SWNTs morphologies

As a general result, we have obtained identical results for the three R.E. tested. We have first inspected the morphologies of the SWNTs and the production yield as a function of the nominal anode R.E./Ni. ratio. The SWNT production rate has been found to be maximum for an anode ratio between 0.2 and 0.5 and to drastically decrease by a factor up to ten out of this composition range. Furthermore, two kinds of tube morphologies have been observed, in various proportions depending on the

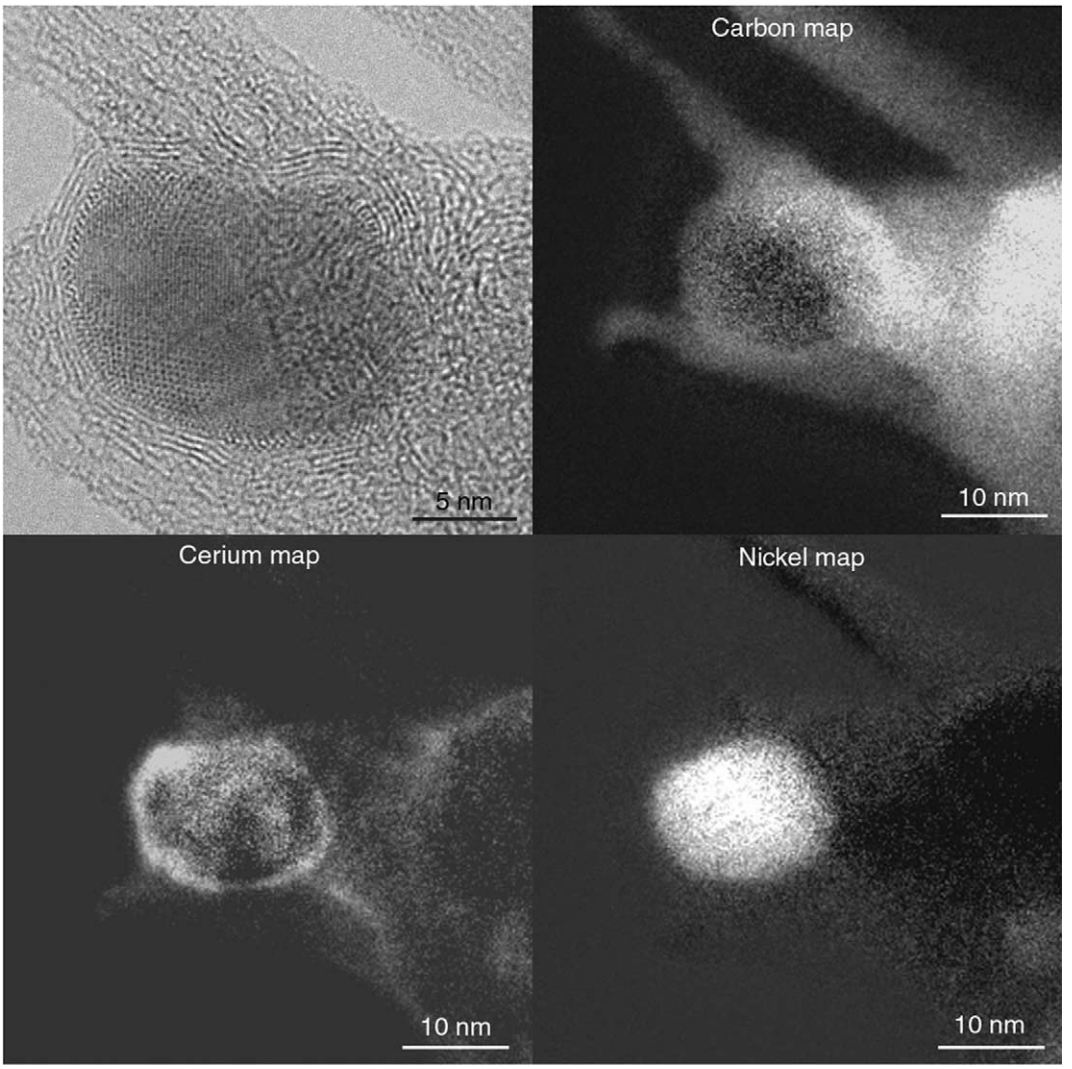

Fig. 8. HRTEM image and C, Ce, Ni chemical maps (EFTEM images at C-Kedge, Ce–$N_{4,5}$ edge and Ni–$M_{2,3}$ edge, Jeol 3010 equipped with a Gatan energy filter (GIF) operating at 300 kV) of a particle linked to long SWNTs ropes in the case of a Ni–Ce catalyst. Ce and C mostly located at the surface of the particle whereas Ni is located in the core of the particle. Furthermore, location of Ce and C is correlated with the observation, in the HRTEM image, of a strong white dot contrast which is not seen in the bulk of the particle and which is the evidence that the surface has a different crystalline structure than the bulk.

anode composition: long ropes as in Fig. 1(a), or sea-urchin-like structures as in Fig. 2(d). Pure Ni produces long ropes only (in low yield) whereas pure R.E. produced sea-urchin structures only. For intermediate anode compositions, both types of tubes are observed in a proportion related to the amount of R.E.

X-ray analysis of the composition of the particles has shown that long ropes are always linked to particles whose composition R.E./Ni is lower than 11 at.% whereas particles of sea-urchin-like structures have a composition R.E./Ni larger than 15 at.% [8]. As a reference, the composition of the particles which are not linked to SWNTs is completely random. Finally, this relationship between particle composition and SWNTs morphologies is found whatever the nominal R.E./Ni anode ratio.

3.3. Particle analyses

It results from this first analysis that the particle structure and composition are crucial parameters to be identified for explaining the differences observed between the SWNT morphologies. Chemical maps, chemical profiles and HRTEM images have been recorded on numerous particles linked either to long ropes or to sea-urchin-like structures.

In the case of long ropes, chemical maps obtained in EFTEM (Fig. 8) and in STEM modes (Fig. 9) reveal that the core of the particle is pure Ni whereas the surface is partially R.E. enriched. Line-scan profiles extracted along a section of the particle in STEM mode provide a clear quantitative evidence of the spatial anticorrelation between Ni and R.E.. R.E. is not uniformly distributed at the surface but is concentrated in thin platelets which are clearly recognised in HRTEM images since they display a contrast different from the core (Fig. 8(a) and Fig. 10). In HRTEM, simply speaking, the contrast of crystalline areas consists of dot patterns which are images of the atomic structure projected along the incident electron beam and where periodicities and symmetries reflect those of the crystal lattice [9]. In our case, the dot pattern linked to R.E. rich platelets exhibit periodicities larger than those present in the core, meaning that the difference in composition has a structural counterpart. Analyses of the different patterns have revealed that the core has the FCC structure of nickel whereas the platelets have the structure of the carbide R.E.C_2 [21] as shown in Fig. 10.

These conclusions are supported by image simulations calculated using the EMS code for the experimental conditions of observation (Fig. 10). The platelets have been found to display two important features: their thickness is in general restricted to 2–3 atomic layers and they are always oriented with their (110) plane parallel to the surface. These peculiarities were taken into account in the simulations. In particular, the projected thickness of the platelet along the electron beam, which is one of the simulation parameters, has been determined from its lateral thickness and from the diameter of the whole particle assumed to be spherical. It is worth noticing that, in these conditions, experimental patterns of both the Ni core and the R.E.C_2 platelet could be faithfully simulated for the same set of microscope operating parameters (the objective defocus, which is the most sensitive one, is indicated in insets of Fig. 10), attesting for the reliability of the analysis.

The identification of the surface platelets is very crucial and provides the key of the SWNT nucleation. Indeed, their presence has been found to be directly related to the nucleation of SWNTs since a direct link between the ropes and the platelets has been frequently observed, as attested in the examples shown in Fig. 11 (see also examples in [21]). In Fig. 11(b) in particular,

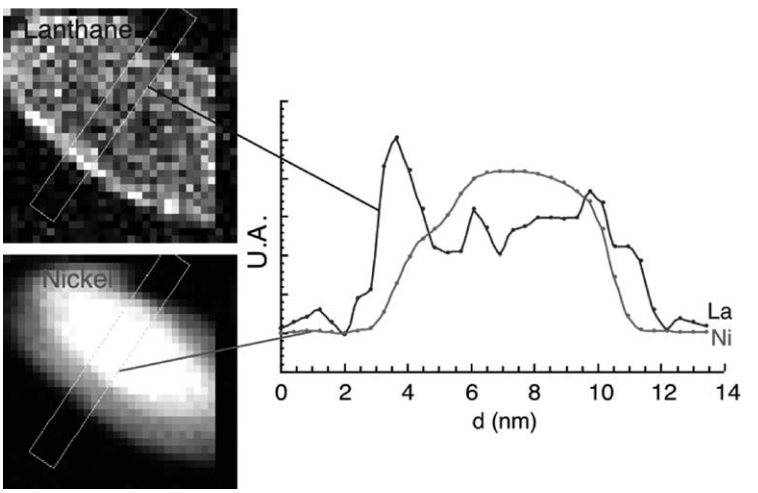

Fig. 9. EELS chemical analysis of a particle obtained with a Ni-La catalyst (STEM –VG501 operating at 100 kV in the 2D-line EELS spectrum mode). Left: spectrum images extracted from line scans at La–$N_{4,5}$ edge and Ni–$M_{2,3}$ edge. Right: chemical profiles extracted along a section of the particle showing that La and Ni are spatially anticorrelated.

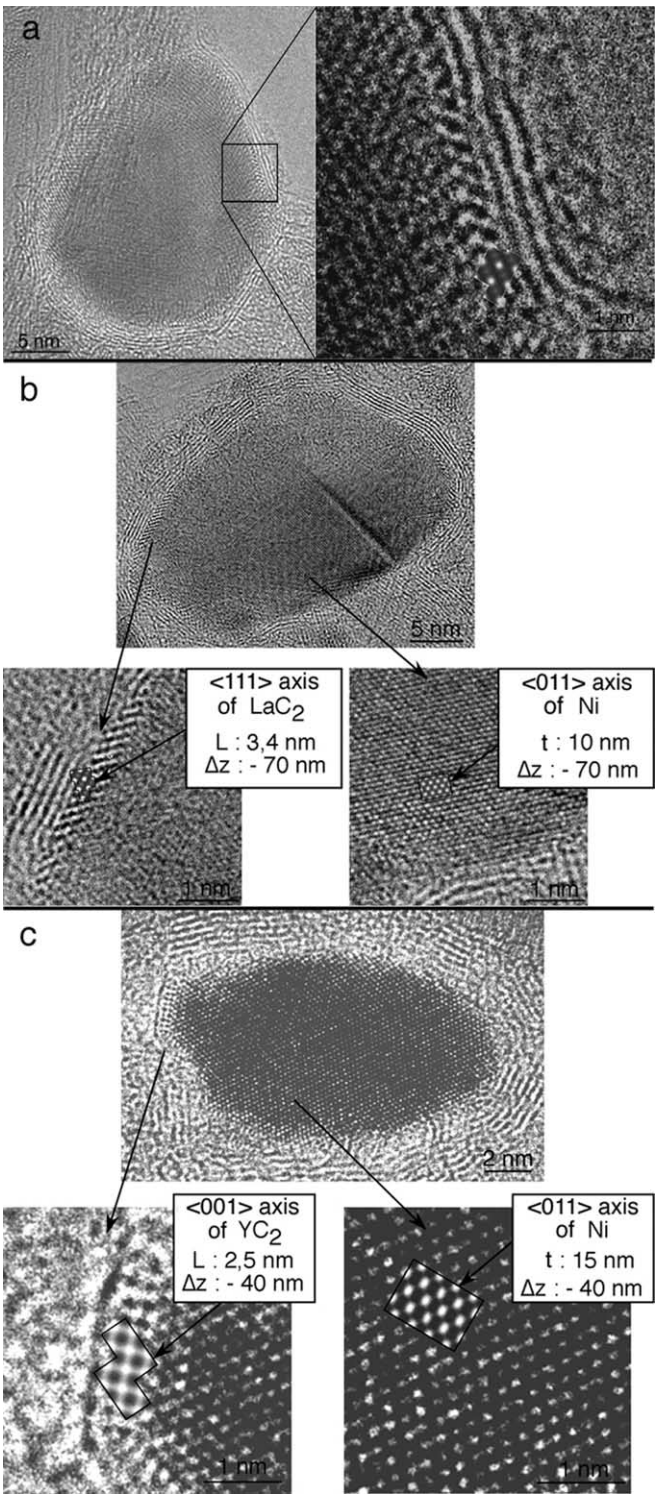

Fig. 10. HRTEM images (Jeol 4000EX) of particles showing a pure FCC Ni core and partially covered by platelets having the structure of the $REMC_2$ carbide: R.E. = Ce in (a), La in (b) and Y in (c). Carbide and Ni are seen as dot patterns which are images of the crystalline lattice. HRTEM simulations of both Ni and carbide are superimposed in the zoomed images. Conditions of simulations are indicated in the insets: Δz is the objective defocus, L the projected thickness of the carbide platelets and t the projected thickness of the Ni crystallite (L and t are both estimated from the shape of the particle).

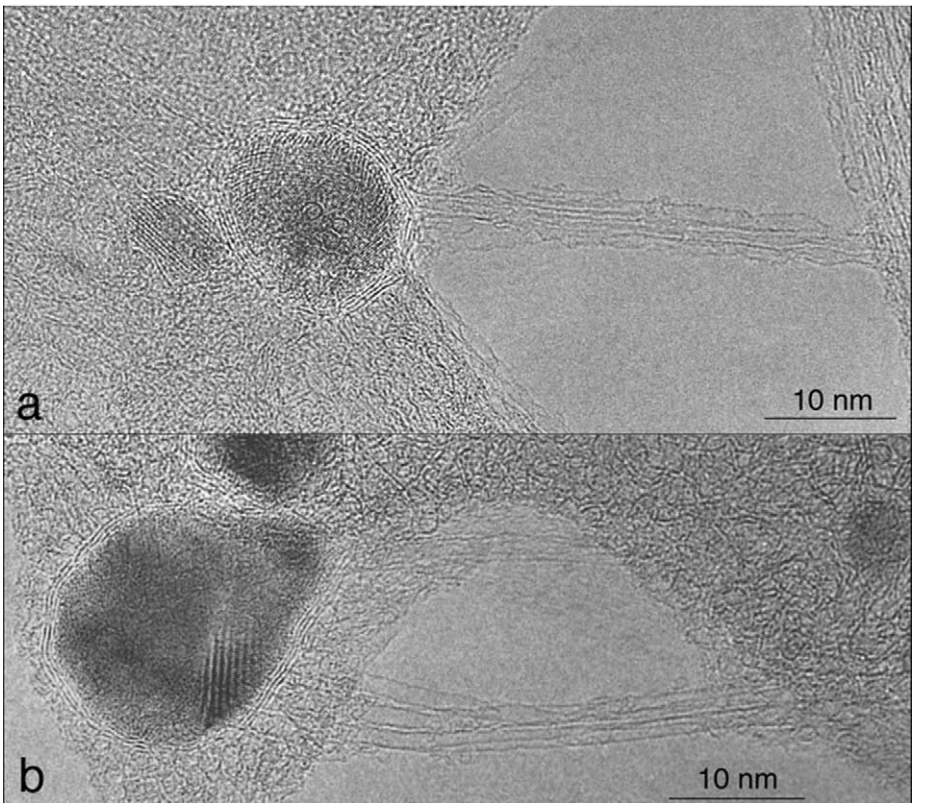

Fig. 11. HRTEM images illustrating the link between the carbide at the particle surface and the roots of the long ropes. In (a), the carbide platelet is edge on, whereas in (b), the carbide platelet is lying at the top of the particle.

the platelet is lying at the top of the particle in the plane of projection so as it is imaged by a fringe contrast and the feet of the SWNTs of the rope are clearly attached at the surface of the platelet.

The particles linked to sea-urchins are different. The same carbides are observed at the surface but now they cover uniformly the surface as a thin shell (2–3 layer thick) encapsulating the particle (Fig. 12). Furthermore, the core is now a complex Ni–R.E.–C compound such as the R.E.NiC_2 compound identified in the example of Fig. 12(b) or the R.E.C_2 carbide itself when the catalyst is 100% R.E. [8,27]. This total higher R.E. concentration is fully consistent with EDX analyses. In addition the core is frequently microcrystalline, which was not the case of pure Ni cores, suggesting rapid solidification due to rapid cooling conditions (Fig. 12(a)).

3.4. Discussion: the catalytic role of rare earth elements

The results presented above can be summarized as follows: the nanotube nucleation is directly linked to the presence of R.E.C_2 carbide at the surface of the particle, the number of nanotubes emerging from it being directly related to the covering of the particle by the carbide layers. Furthermore, the length of the tube is linked to the presence of R.E. in the core: when present, the length remains below 100 nm whereas in the other case there is no limitation in the length nanotubes can achieve.

For explaining the role of the R.E. in the nucleation, one has first to explain the formation of the surface carbide. This results from the combination of two properties of the R.E. metals: their abilities to form a stable carbide, with melting temperatures higher than that of Ni (for example, the melting temperature of YC_2 is equal to 2415 °C) and their low surface energy, which is about ten times lower than that of carbon. This second effect induces a co-segregation of C and R.E. at the particle surface at temperatures higher than the solidification point of the particle. Once at the surface, because of the first effect, R.E. and C self assemble to form a chemically ordered surface layer, which is likely to be seen as a raft floating at the surface of the particle. More precisely, since the carbide layer is experimentally found to always have the (110) orientation, the chemical ordering of the surface layer should resemble the chemical ordering of the (110) plane of the carbide. This plane consists of a regular pattern of carbon pairs and of R.E. atoms (Fig. 13). It is striking that the carbon pair spacing, equal to 0.12–0.13 nm, is very close to the first neighbour distance in the graphene structure. This peculiarity strongly suggests that the carbon pairs can serve

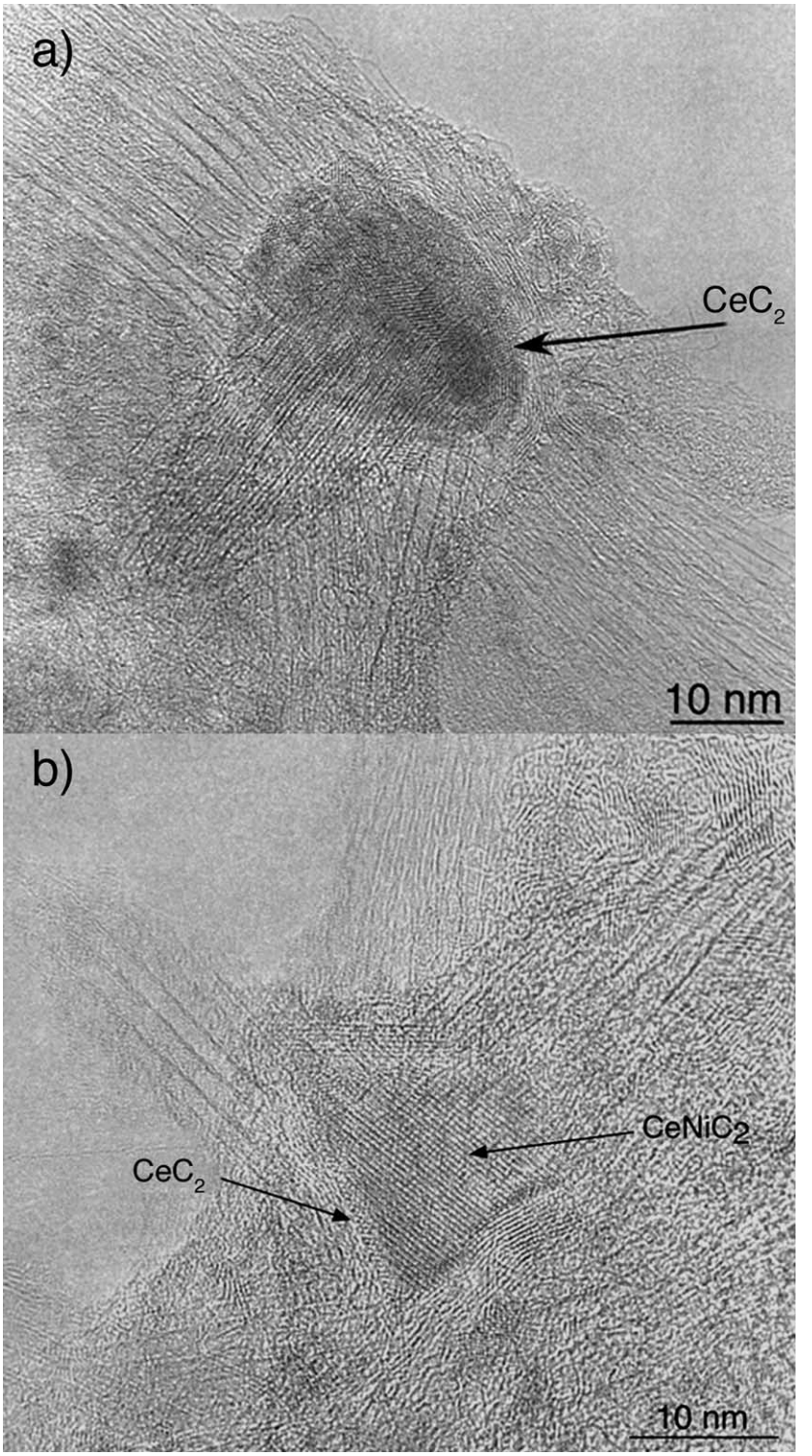

Fig. 12. HRTEM images of metallic particles of a sea-urchin like structure. The catalyst is a Ni–Ce mixture. The particles are homogeneously covered by a shell of CeC_2 carbide whereas the core is most frequently microcrystalline as in a) and its crystalline structure corresponds to complex ternary Ni–Y–C compounds such as $NiYC_2$ identified from the dot pattern in (b).

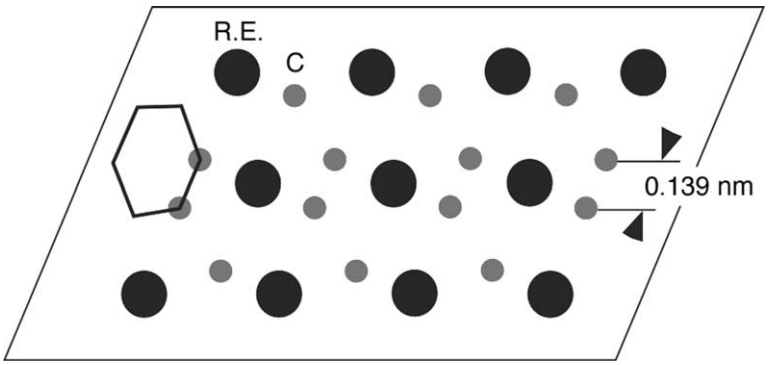

Fig. 13. (110) plane of the body centred tetragonal structure of the rare earth carbides (R.E.)C_2.

as nucleation sites for a graphitic network *perpendicular* to the surface. This would be the starting point for the formation of SWNTs nuclei.

Furthermore, the presence of R.E. atoms mixed with the carbon pairs is thought to help stabilizing SWNTs nuclei, thanks to a third property of R.E., which is the ability to transfer electrons to carbon. This effect has been studied thanks to simulations using a tight binding modeling of C–C interactions combined with Monte Carlo simulations [21]. These calculations have shown that when the number of electrons is increased, which mimics a charge transfer, the graphene sheet is destabilized in favour of configurations involving pentagons and heptagons. These defects introduce local curvatures which are necessary for building a SWNT nucleus linked by the foot to the surface [18,28]. Therefore, it can be inferred from these simulations that charge transfer effect of R.E. plays in favour of the formation of a SWNT nucleus instead of a graphene layer.

In summary, the carbide surface layer can be seen as a diffuse carbon-rich interface between Ni and graphitic carbon where strong metal–carbon bonds are involved which modifies the properties of the surface of Ni in such a way to avoid the wetting of graphene layers. R.E. carbides are thus found to play an important role in the parameters controlling the surface instability responsible for the SWNT nucleation.

The arguments put above make clear that the density of nucleation sites is directly determined by the R.E concentration of the particle. A low concentration gives rise to a partial carbide covering and to a few number of SWNTs assembled into a rope. This corresponds to the first SWNT morphology. On the other hand, a high concentration provides a complete surface covering by the carbide and an isotropic distribution of nucleation sites which results in the sea-urchin structure.

Let us now discuss the difference in length between long ropes and see-urchin structures. As said previously, growth stops when the particle solidifies or when the carbon source is exhausted. If the growth proceeds by the incorporation of carbon via a dissolution-precipitation process as mentioned in Section 2.5, the presence of a continuous carbide layer at the surface, at high concentration of R.E., can act as a poison to the dissolution process since the layer is saturated in carbon. The carbon initially dissolved in the particle is therefore the only feeding source for growth. In addition, the observation that R.E. rich particles are microcrystalline indicates a solidification in a high temperature gradient. Since in situ temperature measurements indicate that higher the temperature higher the local temperature gradient [14], R.E. rich particles are likely to solidify at higher temperature than Ni. At such temperature, due to the corresponding high temperature gradient, the residence time of the particle at temperatures suitable for the growth has been very short. In Ni rich particles, on the contrary, longer residence time can be achieved resulting in extended growth. Both effects – poisoning and rapid solidification – may explain why tubes of sea-urchins remain short whereas, at low R.E. concentration, long tubes are observed.

4. Conclusions

We have presented a review of combined HRTEM, EFTEM and EELs studies which are proved to be powerful and essential tools for identifying and studying the nucleation and growth of single wall carbon nanotubes.

We have shown that whatever the synthesis technique and the tube morphology, SWNTs nucleate and grow from catalyst particles. Depending on the synthesis technique, the tubes are observed to grow *parallel* or *perpendicular* to the surface of the particle. In the former case, observed in CCVD synthesis techniques, the diameter of the tube is correlated to that of the particle which is trapped at the tip of the tube, whereas in the latter case, mostly found in vaporization based synthesis techniques, there is no correlation between the diameter of the tube and that of the particle.

Phenomenological models of nucleation and growth have been discussed with a particular emphasis on the *perpendicular* growth of nanotube bundles since in that case the classical models of growth working for carbon filaments cannot be applied

as they do for the *parallel* growth situation. We have shown that there is now strong experimental evidence in favour of a root growth process where carbon, dissolved at high temperature in catalytic particles, segregates at the surface at lower temperature and forms tubes via a nucleation and growth process.

Particular attention has been paid to the nucleation step where the main problem is to understand why carbon does not always form graphene sheets wrapping the particles. This competition necessarily involves a surface instability where one control parameter is the low surface tension of carbon compared to metal transition.

The origin of this instability has been studied in detail for a particular class of catalyst Ni–R.E. (R.E. = Y, Ce, La) in order to understand why some addition of the R.E. drastically increase the production yield. Thanks to minutest structural and chemical analysis of the particles linked to the tubes, the respective roles of Ni and R.E. have been understood as follows. Ni has the property to dissolve carbon in the liquid state and to reject it in the solid state allowing the graphitization of carbon at temperatures as low as 1400 K. R.E. is a co-catalyst of Ni playing the role of a surfactant. Because of its low surface tension and its ability to form stable carbides, it co-segregates with C at the surface of the particle and forms a chemically ordered surface layer which mimics the structure of the $R.E.C_2$ carbide. This chemical modification of the surface of Ni certainly inhibits its wetting by a graphene sheet and therefore contributes to the nuclation process. In particular, tight binding calculations [21] indicates that a charge transfer of R.E. to carbon should be involved in the destabilization of the graphene sheet in favour to a SWNT nucleus. By modifying the surface activity of Ni, R.E. controls the SWNT nucleation rate.

Many questions remain open, however, such as for instance the extension of the surface arguments identified for the Ni–R.E. class to other classes of catalyst (metal transition mixtures for instance), the nature of the parameter controling the tube helicity and its diameter. . . .

Finally, according to the root growth process, examination of the feet of the tubes and of their interface with metallic particles provide information on the end of the growth and additional proof that SWNT and graphene sheets form for different local conditions. Furthermore, MWNTs are found to be intermediate situations between the two former morphologies.

Acknowledgements

Part of this work has been supported by a TMR contract N° HPRN-CT-2000-00128.

References

[1] C. Journet, W.K. Maser, P. Bernier, M. Lamy de la Chapelle, S. Lefrant, P. Deniard, R. Lee, J.E. Fischer, Nature 388 (1997) 756.
[2] A. Thess, R. Lee, P. Nikolaev, H. Dai, P. Petit, J. Robert, C. Xu, Y. Hee, S.G. Kim, A.G. Rinzler, D.T. Colbert, G.E. Scuseria, D. Tománek, J.E. Fischer, R. Smalley, Science 273 (1996) 483.
[3] W.K. Maser, E. Munoz, R.E. Smalley, A.M. Benito, M.T. Martinez, G.F. de la Fuente, Y. Maniette, E. Anglaret, J.-L. Sauvajol, Chem. Phys. Lett. 292 (1998) 587;
E. Munoz, W. Maser, A.M. Benito, M.T. Martinez, G.F. de la Fuente, A. Righi, J.-L. Sauvajol, E. Anglaret, Y. Maniette, Appl. Phys. A 70 (2000) 145.
[4] D. Laplaze, P. Bernier, W.K. Maser, G. Flamant, T. Guillard, A. Loiseau, Carbon 36 (1998) 685;
L. Alvarez, T. Guillard, J.-L. Sauvajol, G. Flamant, D. Laplaze, Appl. Phys. A 70 (2000) 169.
[5] H. Dai, A.G. Rinzler, P. Nikolaev, A. Thess, D.T. Colbert, R.E. Smalley, Chem. Phys. Lett. 260 (1996) 471.
[6] H.M. Cheng, F. Li Su, G. Pan, H.Y. Pan, L.L. He, X. Sun, M.S. Dresselhaus, Appl. Phys. Lett. 72 (1998) 3282.
[7] J.-F. Colomer, G. Bister, I. Willems, Z. Konya, A. Fonseca, G. Van Tendeloo, J.B. Nagy, Chem. Commun. 14 (1999) 1343;
J.-F. Colomer, C. Stéphan, S. Lefrant, G. Van Tendeloo, I. Willems, Z. Konya, A. Fonseca, C. Laurent, J.B. Nagy, Chem. Phys. Lett. 317 (2000) 83.
[8] J. Gavillet, A. Loiseau, F. Ducastelle, S. Thair, P. Bernier, O. Stéphan, J. Thibault, J.-Ch. Charlier, Carbon 40 (2002) 1649.
[9] Ph. Lambin, A. Loiseau, C. Culot, L.P. Biro, Carbon 40 (2002) 1635.
[10] S. Arepalli, P. Nikolaev, W. Holmes, C.D. Scott, Appl. Phys. A 70 (2000) 125;
C.D. Scott, S. Arepalli, P. Nikolaev, R.E. Smalley, Appl. Phys. A 72 (2001) 573.
[11] A.A. Puretzky, D.B. Geohegan, X. Fan, S.J. Pennycook, Appl. Phys. A 70 (2000) 153.
[12] A.A. Puretzky, H. Schittenhelm, X. Fan, M.J. Lance, L.F. Allard Jr., D.B. Geohegan, Phys. Rev. B 65 (2002) 245425.
[13] F. Kokai, K. Takahashi, M. Yudasaka, R. Yamada, T. Ichihashi, S. Iijima, J. Phys. Chem. B 103 (1999) 4346;
F. Kokai, D. Kasuya, K. Takahashi, M. Yudasaka, S. Iijima, Appl. Phys. A 73 (1) (2001) 40.
[14] N. Dorval, A. Foutel-Richard, M. Cau, A. Loiseau, B. Attal-Trétout, J.L. Cochon, D. Pigache, P. Bouchardy, V. Krüger, K.P. Geigle, J. Nanosc. Nanotech. (2003), in press.
[15] H. Kanzow, A. Ding, Phys. Rev. B 11 (1999) 180;
H. Kanzow, C. Lenski, A. Ding, Phys. Rev. B 63 (2001) 15402.
[16] V.L. Kusnetzov, A.N. Usoltseva, A.L. Chuvillin, E.D. Obratzova, J.-M. Bonard, Phys. Rev. B 64 (2001) 235401.

[17] A. Gorbunov, O. Jost, W. Pompe, A. Graff, Carbon 40 (2002) 113.
[18] A. Maiti, C.J. Brabec, J. Bernholc, Phys. Rev. B 55 (1997) 6097.
[19] J. Gavillet, A. Loiseau, C. Journet, F. Willaime, F. Ducastelle, J.-Ch. Charlier, Phys. Rev. Lett. 87 (2001) 275504.
[20] J.-Ch. Charlier, G.-M. Rignanese, X. Blasé, De Vita, R. Car (2003), unpublished.
[21] J. Gavillet, J. Thibault, O. Stéphan, H. Amara, A. Loiseau, Ch. Bichara, J.-P. Gaspard, F. Ducastelle, J. Nanosc. and Nanotech. (2003), in press.
[22] A. Loiseau, F. Willaime, Appl. Surface Sci. 164 (2000) 227.
[23] J.-L. Cochon, J. Gavillet, M. Lamy de la Chapelle, A. Loiseau, M. Ory, D. Pigache, in: H. Kuzmany, J. Fink, M. Mehring, S. Roth (Eds.), Electronic Properties of Novel Materials Science and Technology of Molecular Nanostructures, American Institute of Physics, 1999, p. 237.
[24] M. Castignolles, A. Foutel-Richard, A. Mavel, J.-L. Cochon, D. Pigache, A. Loiseau, P. Bernier, in: H. Kuzmany, J. Fink, M. Mehring, S. Roth (Eds.), Electronic Properties of Novel Materials Science and Technology of Molecular Nanostructures, American Institute of Physics, 2002, p. 385.
[25] P. Nikolaev, M.J. Brnokowski, R.K. Bradley, F. Rohmund, D.T. Colbert, K.A. Smith, R.E. Smalley, Chem. Phys. Lett. 91 (1999) 313.
[26] Y. Saito, K. Kawabata, M. Okuda, J. Phys. Chem. 99 (1995) 16076;
Y. Saito, M. Okuda, N. Fujimoto, T. Yoshikawa, M. Tomita, T. Hayashi, Jpn. J. Appl. Phys. 33 (1994) 526;
Y. Saito, Carbon 33 (1995) 979.
[27] D. Zhou, S. Seraphin, S. Wang, Appl. Phys. Lett. 65 (1994) 1593.
[28] X. Fan, R. Buczko, A.A. Puretzky, D.B. Geohegan, J.Y. Howe, S.T. Pantelides, S.J. Pennycook, Phys. Rev. Lett. 90 (2003) 145501.
[29] R.T.K. Baker, Carbon 27 (1989) 315.
[30] A. Oberlin, M. Endo, T. Koyama, J. Cryst. Growth 32 (1976) 335.
[31] G.G. Tibbetts, J. Cryst. Growth 66 (1984) 632.
[32] A.N. Andriotis, M. Menon, G.E. Froudakis, Phys. Rev. Lett. 85 (2000) 3193.
[33] H. Kataura, Y. Kumazawa, Y. Maniwa, Y. Ohtsuka, R. Sen, S. Suzuki, Y. Achiba, Carbon 38 (2000) 1691.
[34] R.S. Wagner, W.C. Ellis, Appl. Phys. Lett. 4 (1964) 89.
[35] T.B. Massalski (Ed.), Binary of Phase Alloys Diagrams, ASM International, 1990.
[36] F. Kokai, K. Takahashi, M. Yudasaka, R. Yamada, T. Ichihashi, S. Iijima, J. Phys. Chem. B 103 (1999) 4346;
F. Kokai, D. Kasuya, K. Takahashi, M. Yudasaka, S. Iijima, Appl. Phys. A 73 (2001) 401.
[37] D. Laplaze, L. Alvarez, T. Guillard, J.M. Badie, G. Flamant, Carbon 40 (2002) 1621.
[38] A. Foutel-Richard, Ph.D. Thesis CNAM, Paris, 2003.
[39] O. Jost, A.A. Gorbunov, J. Möller, W. Pompe, A. Graff, R. Friedlein, X. Liu, M.S. Golden, J. Fink, Chem. Phys. Lett. 339 (2001) 297;
O. Jost, A.A. Gorbunov, J. Möller, W. Pompe, X. Liu, P. Georgi, L. Dunsch, M.S. Golden, J. Fink, J. Phys. Chem. B 106 (2002) 2875.
[40] A. Gorbunov, O. Jost, W. Pompe, A. Graff, Appl. Surface Sci. 197–198 (2002) 563.
[41] J.S. Langer, Rev. Mod. Phys. 52 (1980) 1.
[42] A. Zangwill, Physics at Surfaces, Cambridge University Press, 1998.
[43] J.-F. Colomer, L. Henrard, Ph. Lambin, G. Van Tendeloo, Phys. Rev. B 64 (2001) 125425, Eur. Phys. J. B 27 (2002) 111.
[44] S. Bandow, A. Asaka, Y. Saito, A.M. Rao, L. Grigorian, E. Richter, P.C. Ecklund, Phys. Rev. Lett. 80 (1998) 3779.
[45] X. Ishigaki, et al., Appl. Phys. A (2000).
[46] T. Guillard, S. Cetout, L. Alvarez, J.-L. Sauvajol, E. Anglaret, P. Bernier, G. Flamant, D. Laplaze, Eur. Phys. J. B 5 (1999) 251.
[47] A. Loiseau, N. Demoncy, O. Stéphan, in: Tomanek, Enbody (Eds.), Science and Applications of Nanotubes, Kluwer Academic/Plenum, New York, 2000, p. 1.
[48] L. Henrard, A. Loiseau, C. Journet, P. Bernier, Eur. Phys. J. B 13 (2000) 661.